Nasopharyngeal Cancer-Specific Therapy Based on Fusion Peptide-Functionalized Lipid Nanoparticles

Haiming Luo,[†,‡] Lisen Lu,[†,‡] Fei Yang,[†,‡] Liang Wang,[†,‡] Xiaoquan Yang,[†,‡] Qingming Luo,[†,‡] and Zhihong Zhang[†,‡,*]

[†]Britton Chance Center for Biomedical Photonics, Wuhan National Laboratory for Optoelectronics-Huazhong University of Science and Technology, and
[‡]MoE Key Laboratory for Biomedical Photonics, Department of Biomedical Engineering, Huazhong University of Science and Technology, Wuhan 430074, China

ABSTRACT Current treatment of advanced-stage nasopharyngeal carcinoma (NPC) is not satisfactory. Targeted therapies offer hope for extending survival. Here, we developed simple, robust, and NPC-specific therapeutic lipid nanoparticles based on a fusion peptide, α-NTP, made up of an amphipathic α-helical peptide (α-peptide) linked to an NPC-specific therapeutic peptide (NTP). We found that α-NTP not only retained the sub-30 nm nanostructure-controlling ability of the α-peptide but also displayed the enhanced NPC-targeting ability of the NTP, in which the α-peptide accelerated the uptake of the NTP by NPC cells, with a 4.8-fold increase. Following uptake, α-NTP-based lipid nanoparticles (α-NTP-LNs) exerted coordinated cytotoxicity by inducing cell death *via* apoptosis and autophagy. *In vivo* and *ex vivo* optical imaging data showed that systemically administered α-NTP-LNs efficiently accumulated in the NPC xenograft tumor and displayed high contrast between tumor and normal tissues, which was further confirmed by flow cytometry that there had been a 13-fold uptake difference between tumor cells and hepatocytes. More importantly, the therapeutic efficacy of α-NTP-LNs was specific to NPC xenograft formed with 5-8F cells but not to fibrosarcoma xenograft formed with HT1080 cells *in vivo*. The growth of 5-8F tumors was significantly inhibited by α-NTP-LNs, with more than 85% inhibition relative to control groups (*e.g.*, α-NTP and PBS treatment). In a lung metastasis model of NPC, survival was significantly improved by α-NTP-LN treatment. In a word, these excellent properties of α-NTP-LNs worked in sync and synergistically, maximizing the therapeutic efficacy of α-NTP-LNs against NPC and its metastasis.

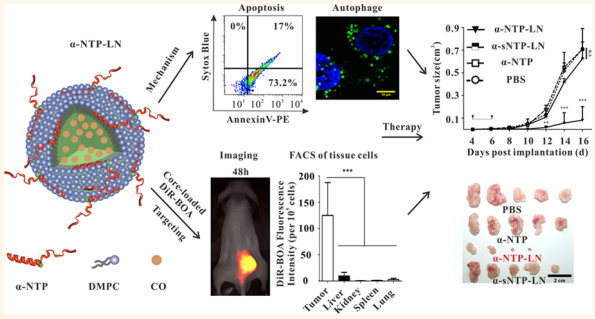

KEYWORDS: peptide · lipid nanoparticles · nasopharyngeal carcinoma · targeted therapy

Nasopharyngeal carcinoma (NPC) is a malignant head and neck cancer that is common in Southern China and Southeast Asia.[1,2] The hidden location and early distant metastasis of NPC are the key reasons for the failure of radiotherapy and chemotherapy treatments.[3] The relative 5 year survival rates of patients diagnosed with NPC in stages I, II, III, and IV are 85.2, 69.4, 44.7, and 37.9%, respectively.[4,5] Targeted therapies (such as monoclonal antibodies) can be beneficial for locally advanced and metastatic cancers, offering hope for increasing survival.[6−8] For example, cetuximab, a chimeric (mouse/human) monoclonal antibody targeting the epidermal growth factor receptor (EGFR), combined with chemotherapy improves the 5 year overall survival of advanced NPC patients, albeit only to a certain extent.[9,10] Thus, it is urgent to develop more efficient NPC-targeting therapeutic strategies.

Nanotechnology has brought a new dimension to targeted cancer therapy due to the potential for increased drug delivery to the tumor as the result of a high drug payload and improved pharmacokinetics and pharmacodynamics.[11,12] Targeted nanoparticles are typically prepared from multiple components, each of which has a distinct function.[13,14] For example, chemotherapeutic drugs are often loaded into the nanoparticle core, which is stabilized with a surface coating and can be further decorated with homing ligands (*e.g.*, peptides, antibodies, aptamers, *etc.*) for active targeting.[15] However, the complex nature of nanoparticle-based therapeutics also brings formidable

* Address correspondence to czyzzh@mail.hust.edu.cn.

Received for review November 19, 2013 and accepted April 26, 2014.

Published online April 26, 2014
10.1021/nn405989n

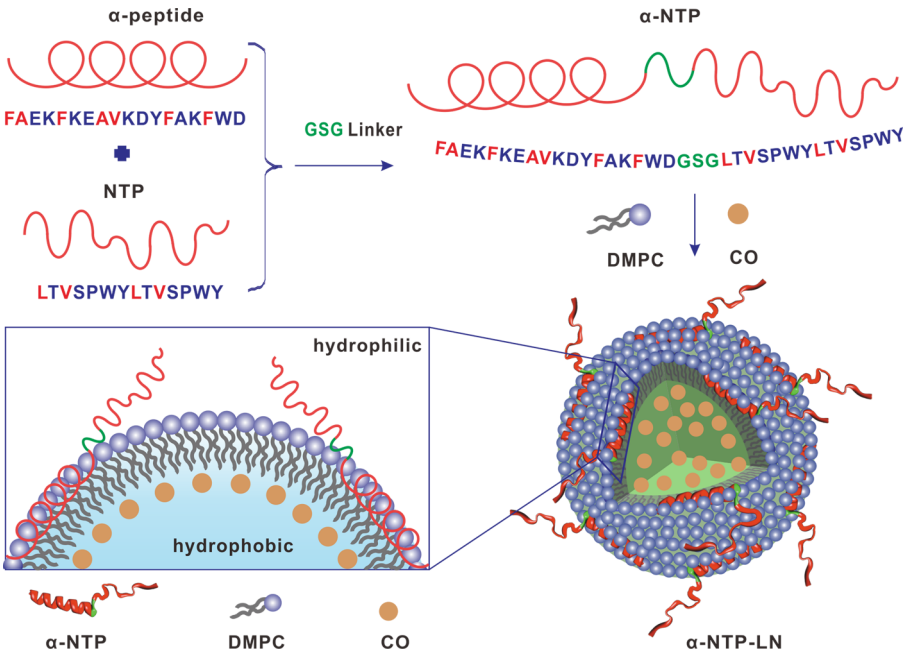

Figure 1. Schematic diagrams of α-NTP and α-NTP-LNs.

hurdles with respect to their clinical translation. These hurdles include the removal of morphological impurities, scaling up, and ensuring batch-to-batch reproducibility.[16,17] Therefore, in addition to efficacy, the key to successful translation of targeted nanomedicines from the bench to the bedside is simplicity.

Here, we report a simple, robust, and selective nanoparticle-based therapeutic approach designed to target and treat nasopharyngeal carcinoma and its distant metastases. As depicted in Figure 1, the key element of this nanoparticle is a fusion peptide sequence, denoted as α-NTP, in which an NPC-specific therapeutic peptide (LTVSPWYLTVSPWY-NH_2, denoted as NTP) is linked to the C-terminus of an amphipathic α-helical peptide (FAEKFKEAVKDYFAKFWD-NH_2, denoted as α-peptide) through a GSG linker. We anticipated that the α-NTP fusion peptide would make the functions of the α-peptide and the NTP intact, with the α-peptide interacting with phospholipids to self-assemble and form stable, spherical nanoparticles and with the NTP guiding the nanoparticles to enter into the NPC cells. The novelty of this approach is based on the following: (1) The NPC-specific therapeutic peptide (the peptide sequence LTVSPWYLTVSPWY) was previously identified in a breast cancer screen,[18,19] and we recently discovered that this peptide has remarkably high *in vivo* specificity for NPC[20,21] and also possesses potent therapeutic activity. (2) The α-peptide (an ApoA-1 mimetic peptide) controls the structure and function of high-density lipoprotein (HDL)-like peptide−phospholipid scaffolds (HPPSs), as demonstrated in our previous studies.[22,23] α-Peptide-based HPPSs are biocompatible spherical nanoparticles with a very small size (~20 nm), a neutral charge, long circulation half-life, and can target scavenger receptor class B1 (SR-B1).[22] (3) SR-B1 is overexpressed in NPC; we recently discovered that SR-B1 is a potential biomarker of NPC and that the growth of this cancer is inhibited by HDL mimetic nanoparticles.[24,25] (4) Thus, this combination of these features creates a perfect scenario in which all elements will work in sync and synergistically, thus maximizing the NPC-specific therapeutic efficacy of α-NTP-based lipid nanoparticles (denoted as α-NTP-LNs).

In this study, we developed the α-NTP-LNs, confirmed their targeting to NPC, verified the synergistic targeting effect of the α-peptide and the NTP in the fusion peptide α-NTP, analyzed the mechanism of α-NTP-LN-induced cell death, and evaluated NPC-specific therapeutic function, particularly the ability to control metastatic NPC *in vivo*.

RESULTS

Fusion Peptide α-NTP Directs Lipid Self-Assembly into Sub-30 nm Nanoparticles. First, we verified that the fusion peptide α-NTP had the ability to control the structure of lipid nanoparticles. α-NTP (0.72 μmol) was added to a lipid emulsion prepared from 1,2-dimyristoyl-*sn*-glycero-3-phosphocholine (DMPC, 3 μmol) and cholesterol oleate (CO, 0.2 μmol), causing the turbid emulsion to become clear. This change strongly suggested that α-NTP decreased the size of lipid aggregates in the emulsion due to formation of smaller α-NTP-LNs, as is the case with α-peptide.[22,26] Fast protein liquid chromatography (FPLC) was used to purify the α-NTP-LNs, and a representative FPLC profile for the α-NTP-LNs showed that the 280 nm absorbance curve had a narrow dominant peak at a retention time of 66.9 min

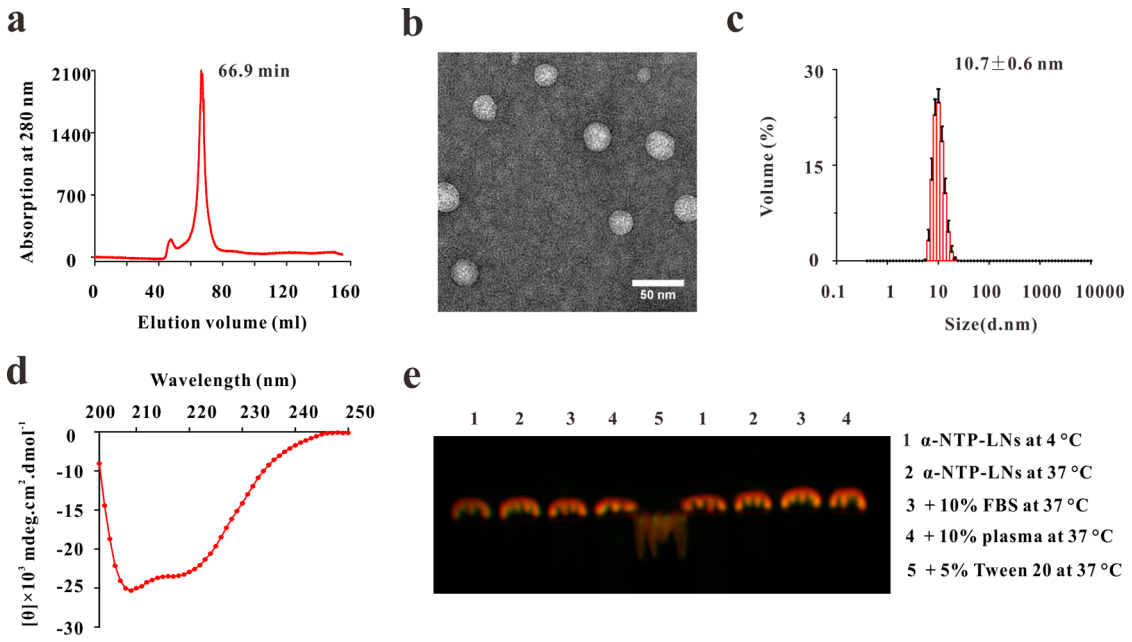

Figure 2. ***In vitro*** **characterization of α-NTP-LNs. (a) FPLC profile of α-NTP-LNs; (b) TEM image of α-NTP-LNs; and (c) size distribution of α-NTP-LNs as determined using DLS. (d) Circular dichroism spectrum of α-NTP-LNs in PBS. (e) Seminative SDS-PAGE assay and fluorescence imaging to evaluate the stability of FITC-(DiR-BOA)α-NTP-LNs.**

(Figure 2a), indicating that the α-NTP induced formation of α-NTP-LNs with a good yield and purity. Transmission electron microscopy (TEM) data showed that the α-NTP-LNs were sub-30 nm nanoparticles with high monodispersity and uniform spherical morphology (Figure 2b). Dynamic light scattering (DLS) data indicated that the size of the nanoparticles was 10.7 ± 0.6 nm ($n = 3$) with a narrow size distribution (Figure 2c). Zeta-potential measurements showed that the α-NTP-LNs were approximately neutral nanoparticles with a zeta-potential of 2.66 ± 0.60 mV ($n = 3$). The circular dichroism spectrum of α-NTP-LNs showed the presence of α-helices, with negative peaks at 222 and 208 nm (Figure 2d).

To measure the stability of α-NTP-LN, we prepared dual-labeled α-NTP-LNs in which α-NTP peptide was labeled with fluorescein isothiocyanate (FITC) and the core was loaded with DiR-BOA (a lipid-anchored near-infrared fluorophore),[26,27] denoted as FITC-(DiR-BOA)α-NTP-LNs. The absorption spectrum of FITC-(DiR-BOA)α-NTP-LNs confirmed that both FITC and DiR-BOA were successfully loaded on the nanoparticles (Supporting Information Figure S1). Fluorescence imaging of seminative SDS-PAGE gels showed both FITC and DiR-BOA fluorescent signals in the same band, indicating that FITC-(DiR-BOA)α-NTP-LNs were stable in 10% FBS and 10% plasma at 37 °C for 3 h. As a control, nanoparticles that were dissociated with 5% Tween-20 showed separation of FITC and DiR-BOA fluorescent signals (Figure 2e; Supporting Information Figure S2). Furthermore, long-term storage stability indicated that α-NTP tightly interacted with the lipids and maintained the stability of nanoparticles (Supporting Information Figure S3).

We also prepared two other types of peptide−lipid nanoparticles as controls. One type was α-peptide-based lipid nanoparticles (denoted as α-LNs). The other type was lipid nanoparticles formed using the fusion peptide α-sNTP, in which the α-peptide is linked to a scramble peptide with the same amino acids as NTP (SYTYSTPVWVPLWL-NH_2, denoted as sNTP) through a GSG peptide linker. FPLC profiles and DLS data showed that both the α-peptide and α-sNTP also efficiently controlled the size of nanoparticles, with sizes of approximately 20 nm (Supporting Information Figure S4). These nanoparticles are denoted as α-LNs and α-sNTP-LNs, respectively.

α-NTP-Based Lipid Nanoparticles Display Strong NPC-Specific Targeting. Second, we verified the ability of α-NTP-LNs to specifically target NPC using confocal microscopy and flow cytometry analysis. α-NTP-LNs core-loaded with DiR-BOA were prepared to investigate the specific uptake of α-NTP-LNs by tumor cells. After 3 h of incubation with (DiR-BOA)α-NTP-LNs, human NPC 5-8F cells displayed a strong fluorescence signal corresponding to DiR-BOA, whereas human fibrosarcoma HT1080 cells excluded (DiR-BOA)α-NTP-LNs (Figure 3a). Flow cytometry data confirmed that the uptake efficiency of (DiR-BOA)α-NTP-LNs was increased in 5-8F cells in a time-dependent manner, and the maximum was almost achieved after 24 h of incubation (Supporting Information Figure S5). The specific targeting ability of α-NTP-LNs was verified by incubating (DiR-BOA)α-NTP-LNs with various cancer cell lines, including a series of NPC cell lines (5-8F, HONE-1, 6-10B, CNE2, CEN1, and SUNE-1), human breast cancer MCF-7 cells, human cervical carcinoma HeLa cells, human

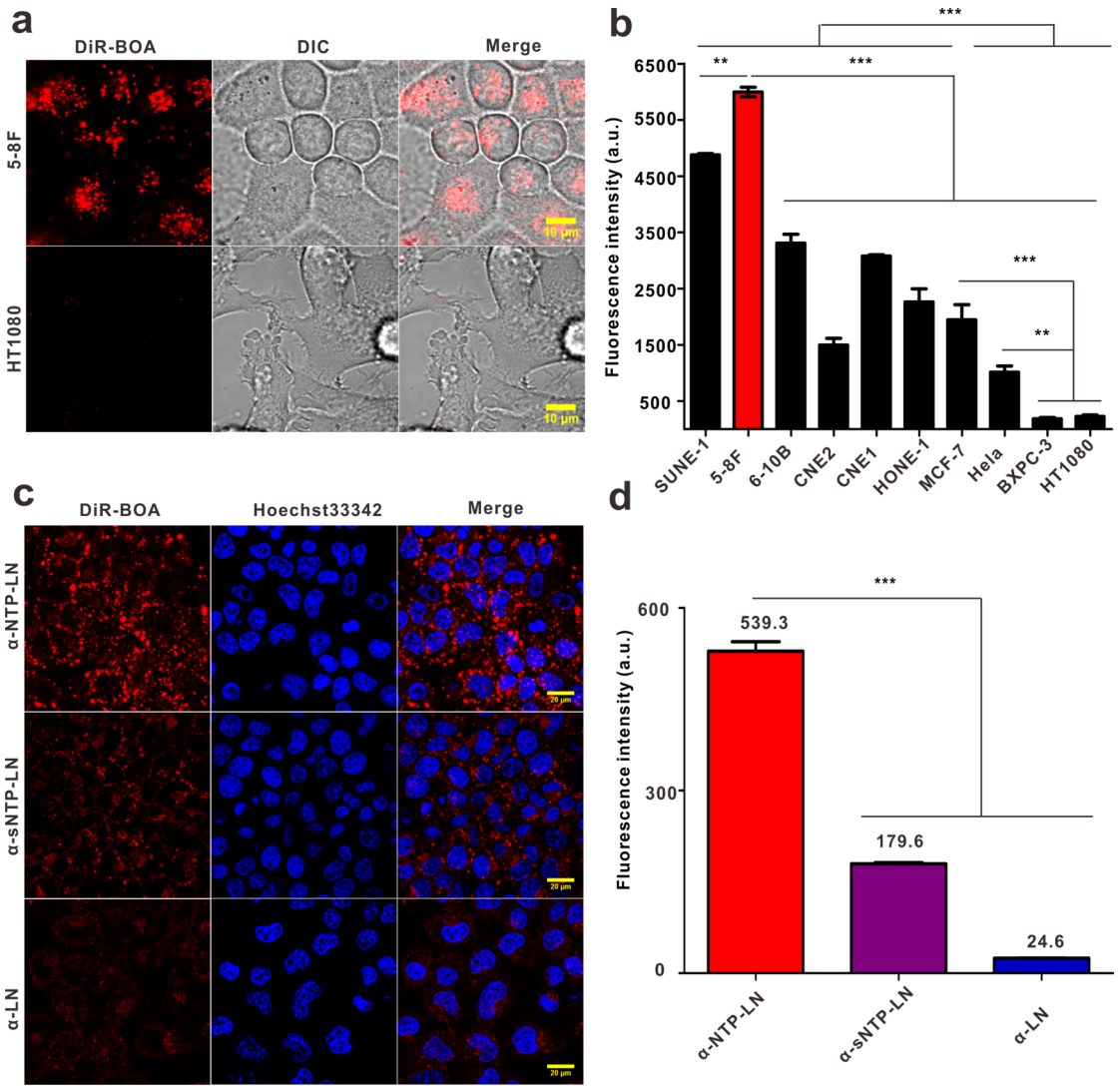

Figure 3. Verification of the NPC targeting of α-NTP-LNs. (a) Confocal images and (b) quantitative flow cytometry analysis of the uptake of (DiR-BOA)α-NTP-LNs by NPC cells (5-8F, HONE-1, 6-10B, CNE2, SUNE-1, and CEN-1) and other tumor cells (MCF-7, HeLa, BxPC-3, and HT1080) that were treated with (DiR-BOA)α-NTP-LNs (2.5 μM peptide concentration) for 3 h. The confocal images are representative images from the positive and negative cells, 5-8F and HT1080 cells, respectively. (c) Confocal images and (d) quantitative flow cytometry analysis of the fluorescence intensity of DiR-BOA in 5-8F cells that were treated with DiR-BOA-loaded α-NTP-LNs, α-sNTP-LNs, or α-LNs (2.5 μM peptide concentration) for 3 h. The data are presented as the mean ± SD (n = 3), **P < 0.01 and ***P < 0.001.

pancreatic carcinoma BxPC-3 cells, and human fibrosarcoma HT1080 cells. As demonstrated by the flow cytometry data shown in Figure 3b, all of NPC cell lines displayed were able to take up the α-NTP-LNs. The 5-8F cells took up the α-NTP-LNs most efficiently, with 3.1-, 5.9-, 32.4-, and 26.8-fold greater uptake than MCF-7 cells, HeLa cells, BxPC-3 cells, and HT1080 cells, respectively (n = 3, P < 0.001). We chose 5-8F cells as the positive control cell line for α-NTP-LN uptake and HT1080 cells as the negative control in the following experiments.

To examine whether the fusion peptide would become dissociated from the nanoparticles upon cellular uptake, 5-8F cells were incubated with FITC-(DiR-BOA)α-NTP-LNs for 3 h at 37 °C. Confocal microscopy showed that 5-8F cells contained both FITC and DiR-BOA signals, and that loss of colocalization indicated that the peptide was released from the nanoparticles (Supporting Information Figure S6). To determine if the NPC-specific targeting of the α-NTP-LNs was due to the NTP or the α-peptide, three types of DiR-BOA-loaded lipid nanoparticles based on α-NTP, α-sNTP, and α-peptide were incubated with 5-8F cells for 3 h. Confocal microscopy and flow cytometry showed that the uptake efficiency of (DiR-BOA)α-NTP-LNs by 5-8F was the highest, which was 21.9-fold greater than (DiR-BOA)α-LNs and 3.0-fold greater than (DiR-BOA)α-sNTP-LNs (Figure 3c,d). These results indicate that the NPC targeting of α-NTP-LNs was mainly due to the influence of NTP. The uptake efficiency of α-sNTP-LNs by 5-8F cells was lower than that of α-NTP-LNs, showing the sequence dependence of the NTP.

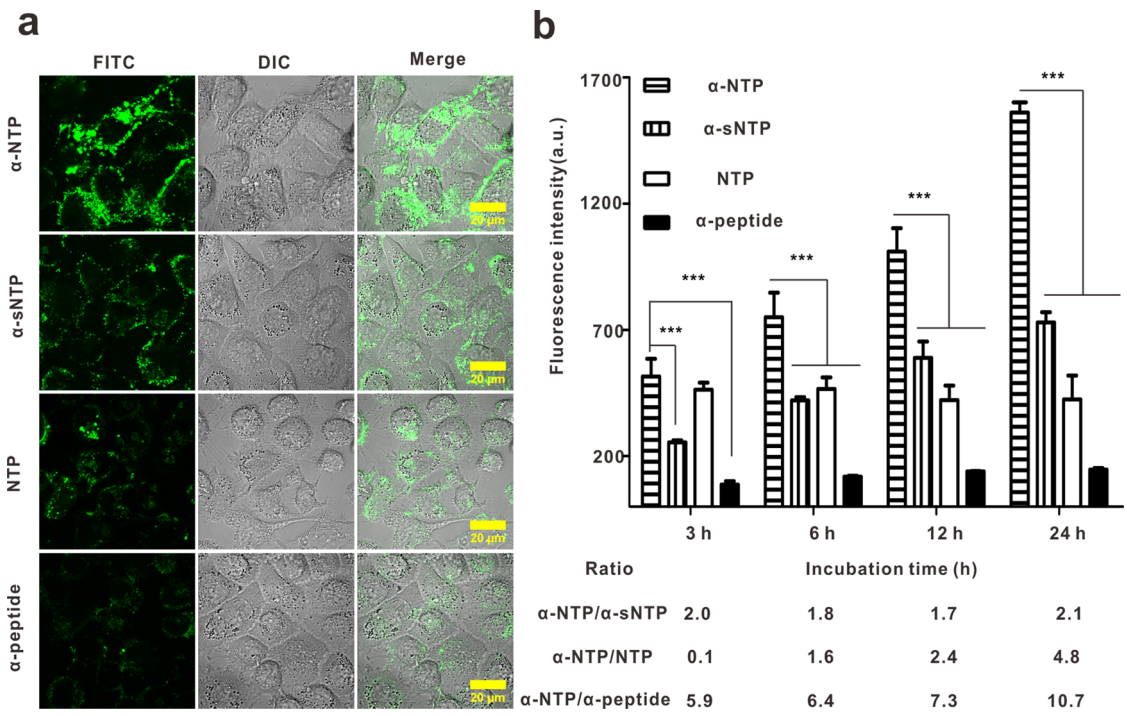

Figure 4. Enhanced NPC-specific targeting ability by linking the NTP and the α-peptide. (a) Confocal imaging of 5-8F cells that were treated with FITC-labeled α-NTP, α-sNTP, NTP, or α-peptide (10 μM peptide concentration) for 24 h. (b) Quantitative flow cytometry analyses of the fluorescence intensity of FITC in 5-8F cells that were incubated with 10 μM FITC-labeled α-NTP, α-sNTP, NTP, or α-peptide for 3, 6, 12, or 24 h. The data are presented as the mean ± SD (n = 3), ***P < 0.001.

α-LNs could also be taken up by 5-8F cells through an SR-B1-mediated uptake pathway.[20,21] However, the α-peptide-mediated uptake of α-LNs by 5-8F cells was much lower than the α-NTP-mediated uptake of α-NTP-LNs. Thus, the fusion peptide α-NTP is responsible for the strong NPC-specific targeting of α-NTP-LNs.

Coordination of the α-Peptide and NTP Enhances the NPC-Specific Targeting of α-NTP. To further analyze the binding of peptides to 5-8F cells and the ability of these cells to take up the peptides, the peptides (α-NTP, α-sNTP, NTP, α-peptide) were labeled with FITC at their N-terminus. In 5-8F cells, confocal imaging showed that all of the peptides entered the cells following 24 h of incubation, and α-NTP accumulated the most (Figure 4a). As shown by flow cytometry (Figure 4b), the uptake of α-NTP, α-sNTP, and α-peptide by 5-8F cells increased in a time-dependent manner, whereas the uptake of the NTP by 5-8F reached saturation early, after 3 h of incubation. We speculated that the α-peptide has the ability to accelerate the entry of the fusion peptide α-NTP into the cells. α-NTP displayed the highest uptake efficiency, which was 5.9- and 10.7-fold greater than that of the α-peptide at 3 and 24 h, respectively. These results show that the enhanced targeting of α-NTP was due to a synergistic effect of the α-peptide and NTP parts of the fusion peptide. We used a scrambled sequence of the NTP to prepare α-sNTP as a control. Uptake efficiency of α-sNTP in 5-8F cells was only ~50% of the efficiency of α-NTP.

Cytotoxicity of α-NTP-LNs Is Associated with Both Apoptosis and Autophagy. Third, we investigated the NPC-specific and concentration-dependent cytotoxicity of α-NTP-LNs. Cell proliferation assays showed that the proliferation rate of 5-8F cells was only 56.6 ± 1.5% when treated with 50 μM (peptide concentration) α-NTP-LNs, whereas the negative control cells, HT1080, were not affected (n = 3, P < 0.001, Figure 5a). When treated with a high concentration (250 μM) of α-NTP-LNs, the proliferation of 5-8F cells was completely inhibited, but HT1080 cell proliferation was only reduced by 21.0 ± 1.7%. The half-maximal inhibitory concentration (IC_{50}) of α-NTP-LNs for 5-8F cells was 61.6 ± 1.5 μM. Flow cytometry analysis confirmed that the death rate of 5-8F cells that had been incubated with nanoparticles for 24 h and then stained with Sytox Blue was correlated to the treatment concentration of α-NTP-LNs, with 93.2 ± 5.6 μM killing half the cells (n = 4, Figure 5b). α-sNTP-LNs and α-LNs induced less than 20% cell death even at a high concentration (250 μM), with no significant difference between α-sNTP-LNs and α-LNs in terms of cytotoxicity to 5-8F cells (n = 4, P > 0.05, Figure 5b). Thus, α-NTP-LNs exerted an effect on NPC 5-8F cells with a half-maximal inhibitory concentration of 62 μM and a half-killing concentration of 93 μM. We were also interested to know how α-NTP-LNs affect tumor cells at a low concentration. The data showed that 50 μM α-NTP-LNs was able to suppress the mobility and colony formation of 5-8F cells (Supporting Information Figures S7 and S8).

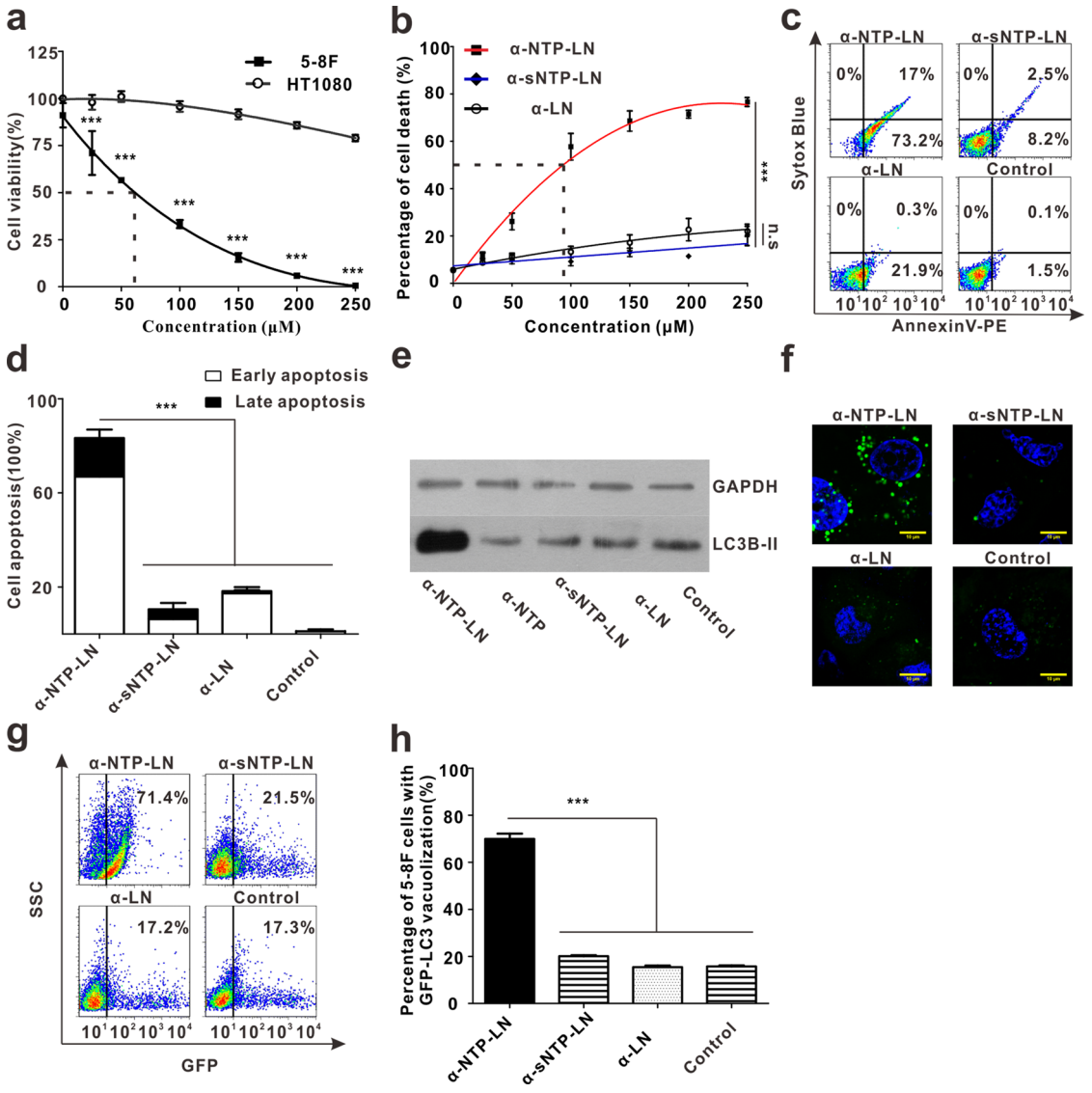

Figure 5. Cytotoxicity assay and analysis of apoptosis/autophagy induced by α-NTP-LNs. (a) Proliferation assays evaluating the cytotoxicity of α-NTP-LNs to 5-8F and HT1080 cells. (b) Quantitative flow cytometric analyses of the mortality rates of 5-8F cells that were treated with α-NTP-LNs, α-sNTP-LNs, or α-LNs for 24 h at different concentrations. (c,d) Quantitative flow cytometric analyses of the cell apoptosis rates of 5-8F cells that were treated with 250 μM α-NTP-LNs, α-sNTP-LNs, α-LNs or PBS for 12 h, in which (c) is the dot plot presentation (Sytox Blue/Annexin V-PE) of representative data and (d) is the column graph of the statistical data from four independent experiments. (e) Western blot analyses of the expression level of LC3B-II in 5-8F cells treated with 250 μM α-NTP-LNs, α-sNTP-LNs, α-LNs, or PBS for 12 h. The expression level of the GAPDH protein was used as the internal reference. (f) Confocal imaging and (g,h) quantitative flow cytometric analyses of GFP-LC3-overexpressing 5-8F cells that were treated with 250 μM α-NTP-LNs, α-sNTP-LNs, α-LNs, or PBS for 12 h, in which (g) is the dot plot presentation (SSC/GFP) of representative data and (h) is the statistical data for the percentage of 5-8F cells with GFP-LC3 vacuolization from three independent experiments. All data are presented as the mean ± SD [(a,h) $n = 3$; (b,d) $n = 4$), ***$P < 0.001$, n.s. = nonsignificant.

To investigate the mechanism of α-NTP-LN-induced cell death, 5-8F cells were incubated with 250 μM α-NTP-LNs, α-sNTP-LNs, and α-LNs for 12 h and then stained with Annexin V-PE and Sytox Blue for flow cytometry analysis (Figure 5c). The data showed that the α-NTP-LNs induced cell death in 83.3 ± 6.2% of cells through the apoptosis pathway, with 66.9 ± 4.5% of cells in early apoptosis and 16.4 ± 3.6% of cells in late apoptosis ($n = 4$, Figure 5d). Only 10.5 ± 3.7% of cells underwent apoptosis in response to α-sNTP-LNs, and 19.2 ± 3.5% of cells underwent apoptosis in response to α-LNs.

We were interested in determining whether the cytotoxicity of α-NTP-LNs was associated with autophagy since some anticancer agents have been reported to synergistically induce autophagy and apoptosis.[28,29] Western blotting was used to analyze the expression levels of microtubule-associated protein 1 light chain 3 beta (LC3B) type II, an important protein marker of autophagic activity,[30,31] in 5-8F cells after 12 h of treatment with α-NTP-LNs, α-sNTP-LNs, and α-LNs. The data showed that the expression level of LC3B-II was very high in 5-8F cells treated with α-NTP-LNs compared with the levels in the control groups (Figure 5e), indicating

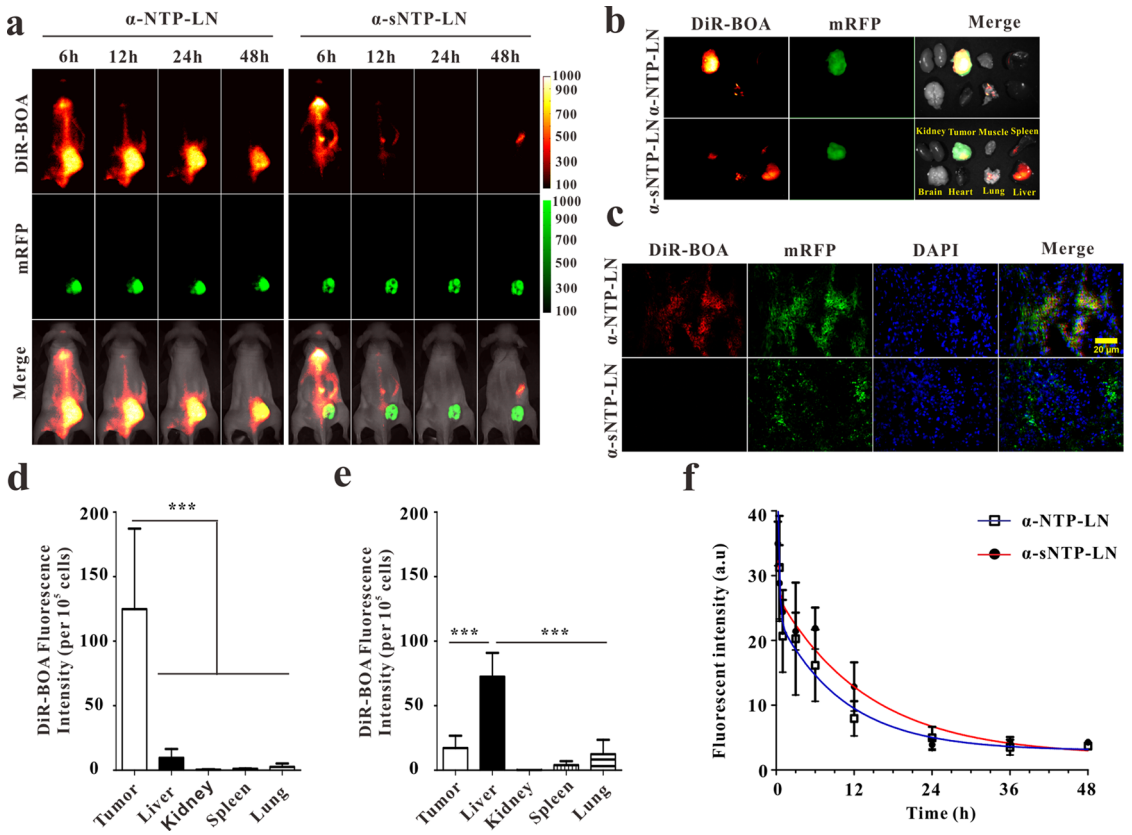

Figure 6. Whole-body fluorescence imaging of α-NTP-LN targeting NPC *in vivo*. (a) Whole-body imaging of mRFP-5-8F tumor-bearing mice 6, 12, 24, and 48 h after the injection of (DiR-BOA)α-NTP-LNs or (DiR-BOA)α-sNTP-LNs. (b) *Ex vivo* images of tumor and normal organs (kidney, muscle, spleen, brain, lung, heart, and liver) removed from mice that were sacrificed 48 h after injection. (c) Fluorescence imaging analyses of the colocalization of DiR-BOA and mRFP in tumor sections that were prestained with DAPI (blue) before multispectral microscopy. (d,e) Histogram of the fluorescence intensity of DiR-BOA-positive cells in tumor tissues and normal organs from tumor-bearing mice injected with (DiR-BOA)α-NTP-LNs (d) or (DiR-BOA)α-sNTP-LNs (e). The data are presented as the mean ± SD from three mice, ***$P < 0.001$. (f) Blood clearance curves of (DiR-BOA)α-NTP-LNs and (DiR-BOA)α-sNTP-LNs in normal mice ($n = 5$).

that α-NTP-LN-induced cell death was associated with autophagy. In addition, green fluorescent protein (GFP)-labeled LC3 was used as a marker to reflect the formation of autophagosomes in the cells.[32,33] Confocal imaging showed that a large number of GFP-LC3 puncta existed in 5-8F cells after 12 h of α-NTP-LN treatment (Figure 5f). Flow cytometry analysis showed that GFP-LC3 was over-expressed in 70.0 ± 2.2% of 5-8F cells treated with α-NTP-LNs, which was much higher than the percentage of cells treated with α-sNTP-LNs (20.1 ± 0.4%), α-LNs (15.4 ± 0.7%), or PBS (15.8 ± 0.4%) ($n = 3$, $P < 0.001$, Figure 5g,h). Thus, α-NTP-LN-induced cell death was associated with both apoptosis and autophagy, which might explain the high efficiency and selective killing of NPC cells by α-NTP-LNs.

Whole-Body Fluorescence Imaging Verification of α-NTP-LN Targeting *in Vivo*. To evaluate the therapeutic efficacy of α-NTP-LNs for 5-8F tumors, we first verified the NPC targeting of these nanoparticles *in vivo* using α-sNTP-LNs as a control. (DiR-BOA)α-NTP-LNs were intravenously injected into monomer red fluorescent protein (mRFP) expressing 5-8F tumor-bearing mice, and the fluorescence signals of the DiR-BOA that had accumulated in the tumor or other tissues were monitored using a homemade whole-body fluorescence imaging system.[20,34,35] At 6 h postinjection, (DiR-BOA)-α-NTP-LNs clearly accumulated in the mRFP-5-8F tumors, whereas few (DiR-BOA)α-sNTP-LNs were present in the tumor (Figure 6a). With increasing time, the (DiR-BOA)α-NTP-LN level in the normal tissues gradually decreased, and these particles selectively accumulated in the tumor regions. However, (DiR-BOA)α-sNTP-LNs still displayed poor tumor accumulation. At 48 h post-injection, the mice were sacrificed to allow for fluorescence imaging to assess the tissue distribution of the nanoparticles and for flow cytometry to analyze the cellular uptake. As shown in Figure 6b, the fluorescence signals for (DiR-BOA)α-NTP-LNs differed greatly between tumor and normal tissues (kidney, muscle, spleen, brain, heart, lung, and liver), whereas (DiR-BOA)α-sNTP-LNs tended to accumulate in the liver.

To assess the penetration ability of (DiR-BOA)α-NTP-LNs in the solid tumor tissue, frozen sections of mRFP-5-8F tumors were imaged using multispectral microscopy (Figure 6c, Supporting Information Figure S9). The imaging data for the tissue slices clearly show

that the fluorescence signal of DiR-BOA colocalized with the mRFP signal in the tumor tissues of (DiR-BOA)α-NTP-LN-injected mice, indicating that the α-NTP-LNs, with an optimal sub-30 nm size, efficiently penetrated the solid tumor and were taken up by the tumor cells. Furthermore, we compared the uptake efficiency of nanoparticles by the cells in tumor and normal tissues using flow cytometry analyses. In the tumor tissue, 46.2 ± 10.1% of the cells were positive for (DiR-BOA)α-NTP-LNs, but only 4.6 ± 3.4% of cells in the liver tissue were positive, and a very low percentage (<2%) of cells in other normal tissues were positive (*e.g.*, kidney, spleen, and lung) (Supporting Information Figure S10). Conversely, the percentage of positive cells that took up (DiR-BOA)α-sNTP-LNs in tumor tissues (9.9 ± 8.3%) was lower than that in liver tissues (45.6 ± 5.3%). Moreover, the fluorescence intensity analysis of the positive cells in tumor and normal tissues indicated that the uptake of (DiR-BOA)α-NTP-LNs by the tumor cells was much higher than the uptake by normal cells in the liver (13.0-fold), kidney (260.7-fold), spleen (115.1-fold), and lung (48.6-fold) (n = 3, P < 0.001, Figure 6d). However, the uptake of (DiR-BOA)α-sNTP-LNs by the tumor cells was only 23.7% of the uptake by hepatocytes, which was also higher than the uptake by normal cells in the kidney (430.2-fold), spleen (31.9-fold), and lung (5.8-fold) (Figure 6e). Thus, *in vivo* fluorescence imaging and flow cytometry analysis indicated that α-NTP-LNs efficiently accumulated in tumor tissues and were selectively taken up by NPC cells.

Furthermore, the blood circulation of nanoparticles was examined in normal BALB/c mice, in which DiR-BOA-loaded α-NTP-LNs and α-sNTP-LNs were intravenously injected, and the fluorescence intensity of DiR-BOA in blood was measured at different time points. As shown in Figure 6f, no significant difference was noted between (DiR-BOA)α-NTP-LNs and (DiR-BOA)α-sNTP-LNs: both blood clearance curves fit the two-compartment model and displayed similar results with calculated half-lives of 9.55 and 429.42 min for (DiR-BOA)α-NTP-LNs and 7.99 and 585.06 min for (DiR-BOA)α-sNTP-LNs. However, rhodamine-B-labeled α-NTP was quickly cleared from the blood circulation with calculated half-lives of 0.49 and 42.73 min (Supporting Information Figure S11). Thus, the prolonged blood circulation time of α-NTP-LNs was beneficial to tumor accumulation.

α-NTP-LNs Inhibited the Growth of 5-8F Tumors but Not HT1080 Tumors *in Vivo*. To evaluate the therapeutic efficacy of α-NTP-LNs when administered systemically, we randomly sorted 5-8F tumor-bearing mice into four groups on the fourth day after tumor cell implantation. The mice were intravenously injected with α-NTP-LNs, α-sNTP-LNs, α-NTP, and PBS on days 4 and 6. The dose of nanoparticles was equivalent to 250 nmol of peptide. Compared with the control treatments, the α-NTP-LNs efficiently inhibited the growth of 5-8F tumors (Figure 7a,b) but did not affect HT1080 tumor growth (Supporting Information Figure S12). On the 16th day, the mean tumor volumes were significantly different between the α-NTP-LN-treated group (82 ± 119 mm^3) and the α-sNTP-LN-treated group (624 ± 85 mm^3), the α-NTP-treated group (708 ± 65 mm^3), and the PBS-treated group (711 ± 179 mm^3) (n = 5, P < 0.001, Figure 7a,b). The growth of 5-8F tumors was inhibited by α-NTP-LNs, with more than 85% inhibition relative to the α-sNTP-LN-, α-NTP-, and PBS-treated control groups. No obvious body weight loss was observed during the treatment in all groups (Supporting Information Figure S13).

To verify the mechanism of tumor growth inhibition by α-NTP-LNs *in vivo*, histological analysis of frozen tumor sections was performed using hematoxylin and eosin (HE) staining, TdT-mediated dUTP nick end labeling (TUNEL), and fluorescence immunohistochemical staining with an LC3B antibody. The results of the HE staining and TUNEL assay confirmed that α-NTP-LNs induced a higher rate of cell apoptosis (53.3 ± 13.3%) in tumor tissues compared with the other treatments, which induced apoptosis in only 18.9 ± 6.7% of cells in α-sNTP-LN-treated tumors, 2.9 ± 2.1% of cells in α-NTP-treated tumors, and 3.6 ± 0.4% of cells in PBS control tumors (n = 3, P < 0.001, Figure 7c,d). Confocal imaging of the sections subjected to fluorescence immunohistochemistry confirmed that α-NTP-LNs induced a large number of autophagosomes in the tumor tissue, and the number of fluorescent antibody-labeled LC3B dots was much higher in the α-NTP-LN-treated tumors than in the α-sNTP-LN-treated tumors (9.3-fold), α-NTP-treated tumors (34.1-fold), and PBS control tumors (103.3-fold) (n = 3, P < 0.001, Figure 7c,e).

To evaluate potential side effects of α-NTP-LNs, blood was collected from the mice on the 16th day of tumor growth for hemanalysis and biochemical analyses. As shown in Supporting Information Figure S14, there were no differences in the hepatic and renal function parameters (*e.g.*, creatinine (Cre), total protein (T-Pro), albumin (Alb), total bilirubin (T-Bil), aspartate aminotransferase (AST), alanine aminotransferase (ALT), urea nitrogen (BUN), uric acid (UA)), and blood hemanalysis parameters (*e.g.*, white blood cells (WBC), blood platelets (PLT), leukocytes (LYM), monocytes (MON), granulocytes (GRA), red blood cells (RBC), hemoglobin (HGB), corpuscular volume (MCV), mean corpuscular hemoglobin concentration (MCHC), red blood cell volume distribution width (RDW)) among the four treatment groups (5 mice per group), indicating that the systemic administration of α-NTP-LNs had few side effects. Thus, these nanoparticles appear to be safe for use *in vivo*.

α-NTP-LNs Delayed NPC Lung Metastasis. To further evaluate the therapeutic efficacy of the systemic (i.v.)

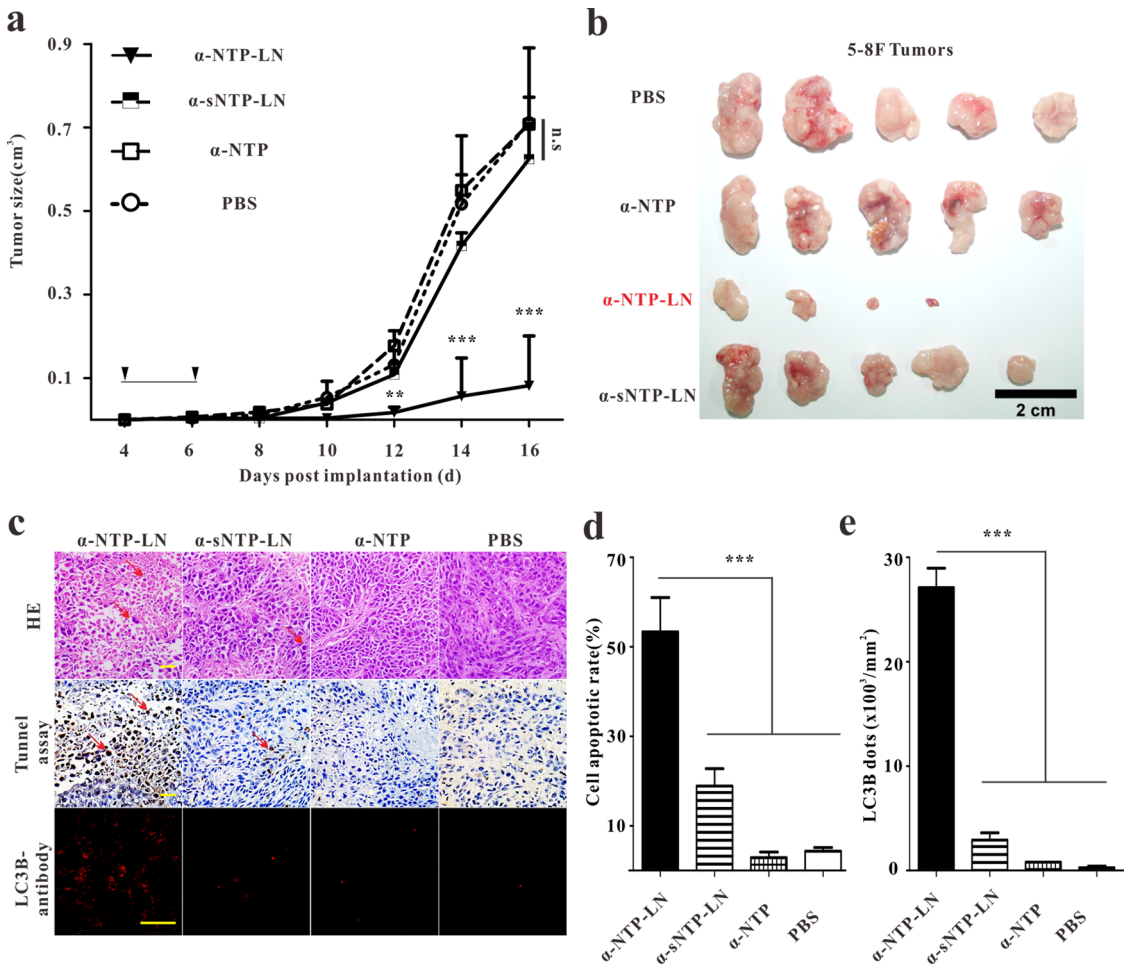

Figure 7. α-NTP-LNs inhibits 5-8F subcutaneous tumor growth. (a) Tumor volume in each group over time. The tumor volume in the α-NTP-LN-treated group was significantly smaller than those of the other groups. The data are presented as the mean ± SD from five mice, **$P < 0.01$, ***$P < 0.001$. (b) Photographs of the tumors from each group on day 16. (c) Histopathological and immunohistochemical analyses of 5-8F tumor tissues from the mice treated with α-NTP-LNs, α-sNTP-LNs, α-NTPs, or PBS. Top row: HE staining. Middle row: TUNEL assay. Bottom row: fluorescence immunohistochemical staining with an LC3B antibody. Scale bars = 20 μm. (d,e) Quantitative analyses of the apoptotic rate (d) and LC3B puncta (e) from (c). The data are presented as the mean ± SD from three tumors, ***$P < 0.001$.

administration of α-NTP-LNs for the treatment of NPC metastasis, we prepared an NPC lung metastasis model through the tail vein injection of 5-8F cells (Supporting Information Figure S15). On days 8 and 10 after 5-8F cell injection, α-NTP-LNs containing 250 nmol of peptide were administered to the tumor-bearing mice *via* tail vein injections. To verify the ability of α-NTP-LNs to control metastasis, the mice were sacrificed on day 45. The necropsy results showed a large number of macroscopic malignant nodules in the PBS control mice and only a few macroscopic malignant nodules in the α-NTP-LN-treated mice. These nodules were confirmed to be malignant by HE staining (Figure 8a). To evaluate the effect of α-NTP-LNs on the survival rate of lung-metastasis-bearing mice, α-NTP-LNs, α-sNTP-LNs, or α-NTPs were intravenously injected into the mice with an equalivalent amount of 250 nmol peptide on days 8 and 10 after 5-8F cell injection. The mice were monitored until day 75 after tumor cell injection, when all of the PBS-treated control mice (n = 9), α-sNTP-LN-treated mice (n = 5), and α-NTP-treated mice (n = 5) had died before day 61 (no significant difference among the three control groups), whereas five of the α-NTP-LN-treated mice were still alive at this time point (n = 9, $P < 0.01$, Figure 8b). Thus, the α-NTP-LNs significantly delayed the development of lung metastases from NPC cells and extended the survival rate of the mice.

DISCUSSION

To meet the need for NPC-targeted therapeutics, we developed a simple and biocompatible lipid nanoparticle system based on the NPC-specific therapeutic peptide α-NTP. Systemic administration of α-NTP-LNs provides an efficient NPC-specific therapeutic strategy, which not only inhibited the growth of NPC but also extended the survival rate of the mice with metastastic NPC *in vivo*.

First, based on the lipid nanostructure-controlling ability of the α-peptide (FAEKFKEAVKDYFAKFWD-NH_2)

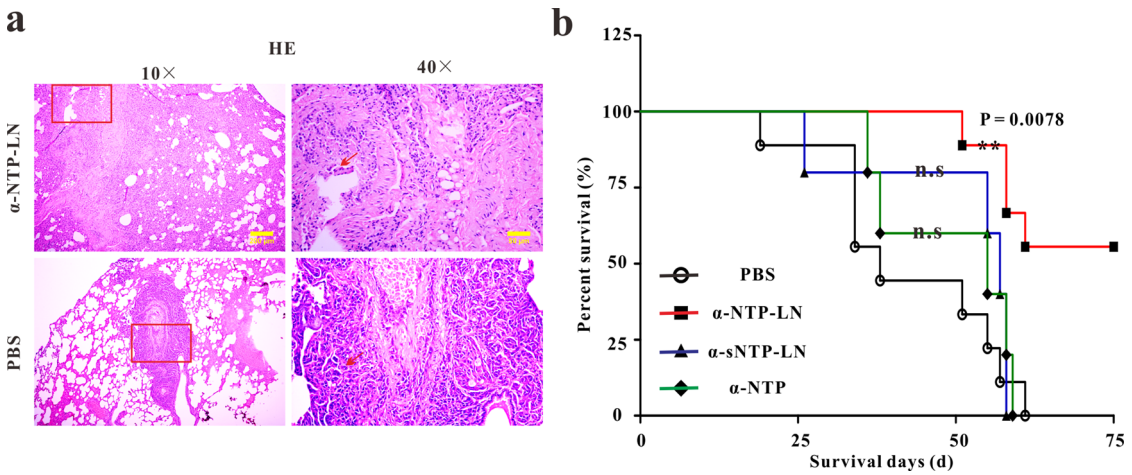

Figure 8. α-NTP-LNs delay progression of NPC lung metastasis. (a) Histopathological analyses of HE-stained lung tissues from α-NTP-LN-treated mice and PBS-treated control mice 45 days after 5-8F cell injection. The images are a representative of those of three mice. (b) Survival curves of mice with NPC lung metastases treated with α-NTP-LNs (n = 9), α-sNTP-LNs (n = 5), α-NTP (n = 5), and PBS (n = 9).

and the NPC-specific targeting ability of the NTP (LTVSPWYLTVSPWY-NH_2), we designed the fusion peptide α-NTP, in which the NTP is linked with the C-terminus of the α-peptide through a GSG linker. Our data verified that α-NTP self-assembled with phospholipids to form α-NTP-LNs, spherical and neutral nanoparticles with a very small size (<30 nm) (Figure 2). All NPC cell lines could efficiently take up α-NTP-LNs, and there was a substantial difference in uptake ability between 5-8F and HT1080 cells (26.8-fold) and between 5-8F and BxPC-3 cells (32.4-fold) (Figure 3b). However, when the NTP was linked to the N-terminus of α-peptide to form the fusion peptide LTVSPWYLTVSPWY-*GSG*-FAEKFKEAVKDYFAKFWD-NH_2, the functions of both the α-peptide and the NTP were lost. The hydrophobic amino acid phenylalanine (F) in the N-terminus of the α-peptide probably led the NTP to be located on the hydrophobic side of the phospholipids, and thus, the fusion peptide was not able to control the size of the lipid emulsions and might not display its targeting function (Supporting Information Figure S16).

Second, the coordination of the α-peptide and the NTP led to the enhanced NPC-specific uptake of α-NTP-LNs. The target of α-peptide-based lipid nanoparticles is SR-B1.[36−38] SR-B1 is highly expressed on NPC cells,[24,39] and NPC cells selectively take up the NTP.[20,21] As predicted, the α-peptide not only controlled the size of the lipid nanoparticles but also accelerated the selective uptake of α-NTP by NPC cells, with 10.7-fold enhancement relative to the α-peptide and 4.8-fold enhancement relative to the NTP (Figure 4b). This synergic effect was confirmed by the 21.9-fold greater uptake efficiency of (DiR-BOA)α-NTP-LNs relative to (DiR-BOA)α-LNs (Figure 3d). The enhanced uptake efficiency is the key factor mediating the NPC-specific cytotoxicity of α-NTP-LNs, as the NPC cell death rate was positively correlated with the concentration and uptake amount of α-NTP (Figure 5a,b and Supporting Information Figure S17).

The coordinated effects of apoptosis and autophagy induced by α-NTP-LNs increased the cell death rate in α-NTP-LN-treated NPC cells (Figure 5) and tumor-bearing mice (Figure 7). Although the scrambled NTP in α-sNTP was used as a control, it only partially decreased (~50%) uptake by NPC cells compared with α-NTP (Figure 4). However, the cytotoxicity of α-sNTP-LNs was much lower than that of α-NTP-LNs (Figure 5b) because α-sNTP-LNs induced low levels of cell apoptosis (Figure 5c,d) and autophagosome generation (Figure 5e−h). These results indicate that the scrambled sequence of the NTP mainly mitigated the cytotoxic effect on positive cells. Furthermore, as shown in Figure 6, there was a substantial difference in the level of α-NTP-LN accumulation between the NPC tumor tissues and normal tissues, and these nanoparticles were selectively taken up by NPC cells, with a 13.0-fold difference between tumor cells to hepatocytes *in vivo*. This selective uptake mediated the NPC-specific therapeutic efficacy of α-NTP-LNs (Figure 7a,b) and delayed the metastasis of NPC (Figure 8).

CONCLUSIONS

In summary, we developed a simple, robust, and highly selective therapeutic lipid nanoparticles, α-NTP-LNs, that exhibited a promising therapeutic effect on NPC tumors and metastases. These effects were due to multiple elements working in sync and synergistically, as follows: (1) the coordinated function of the α-peptide and the NTP to maintain the size of the nanoparticles below 30 nm and enhance the selective uptake by NPC cells, respectively; (2) coordinated cytotoxicity through both apoptosis and autophagy, increasing the cell death rate of NPC cells; and (3) efficient tumor accumulation, with high contrast between tumor and normal tissues due to the

selective uptake by NPC cells, thus preventing side effects. Therefore, the NPC-specific therapy approach developed here maximized the therapeutic efficacy of the NPC-specific therapeutic peptide NTP.

MATERIALS AND METHODS

Materials. 1,2-Dimyristoyl-*sn*-glycero-3-phosphocholine (DMPC) was purchased from Avanti Polar Lipids Inc. (Alabaster, AL, USA). Cholesterol oleate (CO), Hoechst 33342, and the anti-LC3B antibody were obtained from Sigma-Aldrich Co. (St. Louis, MO, USA). DiR-BOA was synthesized according to our previously described procedure.[26,27] Annexin V-PE, Sytox Blue nucleic acid stain, and Alexa Fluor 594 goat anti-rabbit IgG were purchased from Molecular Probes (Carlsbad, CA, USA). Free α-peptide, α-NTP, α-sNTP, and NTP with and without FITC labeling were ordered from Shanghai Apeptide Co., Ltd. (Shanghai, China).

Preparation of α-NTP-LNs, α-sNTP-LNs, and α-LNs. A mixture of DMPC (3 μM) and CO (0.2 μM) in chloroform was dried under nitrogen to form a uniform lipid film. Phosphate-buffered saline (PBS) (1 mL) was added, and then, the mixture was sonicated at 48 °C for 1 h to form the lipid emulsion. To prepare the peptide-based lipid nanoparticles, PBS containing 0.72 μmol of α-NTP, α-sNTP, or α-peptide was added into the lipid emulsion, which was then stored at 4 °C overnight. The nanoparticles were purified using a fast protein liquid chromatography system with a HiLoad 16/60 Superdex 200 pg column (General Electric Healthcare, NY, USA) and concentrated using a concentrator tube with a 30 kDa molecular weight cutoff (Millipore, USA). The protein content of the nanoparticles was quantified using an mp06667-CBQCA protein quantitation kit (Invitrogen Corporation, USA).

Morphology and Size Measurement. The morphology and size of the α-NTP-LNs were evaluated using a Tecnai G^2 20 U-Twin transmission electron microscope (FEI Company, USA). The particle size distributions and zeta-potentials of the nanoparticles were measured using dynamic light scattering (photon correlation spectroscopy) on a Zetasizer Nano-ZS90 system (Malvern Instruments, Worcestershire, UK).

Circular Dichroism. The circular dichroism spectrum of the nanoparticles was measured using a Jasco J-810 circular dichroism spectropolarimeter (Tokyo, Japan) from 200 to 250 nm.

Preparation of Fluorescent Dye-Labeled α-NTP-LNs. To prepare the nanoparticles that were core-loaded with DiR-BOA, the only difference in the previously described protocol was the first step, in which DiR-BOA was mixed with DMPC and CO in chloroform. To prepare FITC-(DiR-BOA)α-NTP-LNs, fluorescein isothiocyanate was conjugated to the lysine residues of the peptides after the (DiR-BOA)α-NTP-LNs was prepared.

Stability Evaluation. The stability of the nanoparticles was evaluated using dual-labeled α-NTP-LNs and seminative SDS-polyacrylamide gel electrophoresis (SDS-PAGE). FITC-(DiR-BOA)-α-NTP-LNs were run in 8% seminative SDS-PAGE gels after a 3 h incubation at 37 °C with PBS, 10% FBS, 10% plasma, and 5% Tween-20. A custom-made optical fluorescence imaging system was used to detect whether the fluorescent band of FITC matched with DiR-BOA.

Cell Culture. Human nasopharyngeal cancer cells (5-8F, HONE-1, 6-10B, CNE2, CEN1, and SUNE-1) were gifts from Prof. Yi-Xin Zeng and Prof. Mu-Sheng Zeng (Sun Yat-sen University Cancer Center, Guangzhou, China). 5-8F cells stably expressing monomer red fluorescent protein were screened out for whole-body fluorescence imaging of the tumor model.[40] Human fibrosarcoma HT1080 cells, human cervical carcinoma HeLa cells, human breast cancer MCF-7 cells, and human pancreatic carcinoma BxPC-3 cells were purchased from the China Center for Type Culture Collection (Wuhan University, Wuhan, China). Human nasopharyngeal cancer cells, mRFP-5-8F cells, and HT1080 cells were cultured in RPMI-1640 (Invitrogen Life Technologies, Carlsbad, CA, USA) supplemented with 10% fetal bovine serum (FBS, Life Technologies), 100 U/mL penicillin, 0.1 mg/mL streptomycin, and 2 mM glutamine in a humidified atmosphere of 5% CO_2 and 95% air at 37 °C. HeLa cells and MCF-7 cells were grown in Dulbecco's modified Eagle medium (DMEM, Life Technologies) containing 10% newborn calf serum (NCS, Life Technologies) at 37 °C in a 5% CO_2 incubator.

Confocal Imaging. The 5-8F and HT1080 cells were seeded into 8-well cover glass-bottom chambers (1×10^4/well; Lab-Tek II Chambered Coverglass; Thermo Scientific, Holtsville, NY, USA) for confocal microscopy. DiR-BOA-loaded nanoparticles (peptide concentration, 2.5 μM) were incubated with cells at 37 °C for 3 h. Before confocal imaging, the cells were stained with or without Hoechst 33342 for 5 min and then washed twice with PBS. The fluorescence signals of the cells were observed using an Olympus FV1000 laser confocal scanning microscope (Olympus, Tokyo, Japan) at excitation wavelengths of 405 nm for Hoechst 33342 and 633 nm for DiR-BOA. FITC-labeled peptides (peptide concentration, 10 μM) were incubated with 5-8F cells at 37 °C for 24 h. The fluorescence signals of the cells were observed using a Nikon A1 MP laser scanning confocal microscope (Nikon, Tokyo, Japan) with an excitation wavelength of 488 nm.

Flow Cytometry Analysis. The cells were seeded into 96-well plates (2×10^4/well) for flow cytometry. DiR-BOA-loaded nanoparticles (2.5 μM) were incubated with cells at 37 °C for 3 h. FITC-labeled peptides (10 μM) were incubated with the cells at 37 °C for 3, 6, 12, or 24 h. Before flow cytometry analysis, the cells were washed three times with PBS. The fluorescence intensity of cells was examined using a microcapillary flow cytometer (Guava EasyCyte8HT, EMD Millipore Corporation, Billerica, MA, USA) with an excitation wavelength of 640 nm for DiR-BOA (785/70 emission filter) and 488 nm for FITC (525/30 emission filter).

Cell Proliferation Assay. The 5-8F cells and HT1080 cells were seeded into 96-well plates at a density of approximately 10 000 cells per well. The cells were treated with α-NTP-LNs at various concentrations (25, 50, 100, 150, 200, 250 μM) for 24 h. The cells were treated with PBS as a control. The cells were washed twice with PBS to remove the nanoparticles and then continuously incubated for 24 h. The cell viability was assessed by the methyl tetrazolium salt assay (Cell Titer 96TM Aqueous; Promega, Madison, WI, USA).

Cell Death Assay. The 5-8F cells were grown in 96-well plates at a density of approximately 20 000 cells per well. Various concentrations (25, 50, 100, 150, 200, 250 μM) of α-NTP-LNs, α-sNTP-LNs, or α-LNs were added to each well, and then, the cells were incubated for 24 h. The 5-8F cells were treated with PBS as a control. The cells were stained with 0.5 μM Sytox Blue (Molecular Probes, Carlsbad, CA, USA) for 30 min, and the cell death rate was quantitatively analyzed using a microcapillary flow cytometer with an excitation wavelength of 488 nm and a 525/30 emission filter.

Apoptosis Detection. The 5-8F cells were treated with 250 μM (peptide concentration) α-NTP-LNs, α-sNTP-LNs, or α-LNs for 12 h. The 5-8F cells were treated with PBS as a control. All of the cells were stained with Annexin V-PE/Sytox Blue and analyzed using a microcapillary flow cytometer with an excitation wavelength of 488 nm for Sytox Blue (525/30 emission filter) and Annexin V-PE (583/26 emission filter). The cells in the lower right quadrant were Annexin V positive and Sytox Blue negative and corresponded to early apoptotic cells. The cells in the upper right quadrant were Annexin V positive and Sytox Blue positive and corresponded to late apoptotic cells.

Autophagy Analysis. The plasmid *GFP-LC3* was constructed by Dr. Liang Wang in our lab[32] using the *LC3* cDNA from *mRFP-LC3*, which was provided by Nicholas T. Ktistakis.[41] After 12 h of transfection with *GFP-LC3*, 5-8F cells were treated with 250 μM (peptide concentration) α-NTP-LNs, α-sNTP-LNs, or α-LNs for 12 h. The cells were treated with PBS as a control. The fluorescence images of cells were observed using a Zeiss LSM 710 inverted confocal microscope (Carl Zeiss, Jena, Germany) equipped with a 63× water immersion objective and a 488 nm excitation

wavelength. The number of cells with GFP-LC3 autophagic vacuoles was quantitatively analyzed using a microcapillary flow cytometer with an excitation wavelength of 488 nm and a 525/30 emission filter.

Western Blotting. The 5-8F cells were treated with 250 μM (peptide concentration) α-NTP-LNs, α-LNs, α-sNTP-LNs, and peptide α-NTP at 37 °C for 12 h. The cells were treated with PBS as a control. The cells were lysed with RIPA lysis buffer (Beyotime, China) and then centrifuged at 12 000 rpm for 5 min. The resultant supernatants were subjected to SDS-PAGE and immunoblotting. Western blotting for LC3B protein was performed as described[32] with a rabbit anti-LC3B antibody (1:1000; Sigma-Aldrich, USA) and a horseradish peroxidase-conjugated anti-rabbit secondary antibody (1:8000; ProteinTech, Wuhan, China). As an internal reference, glyceraldehyde 3-phosphate dehydrogenase (GAPDH) was detected with a mouse anti-GAPDH antibody (1:2000; ProteinTech, Wuhan, China) and a horseradish peroxidase-conjugated anti-mouse secondary antibody (1:8000; ProteinTech, Wuhan, China).

***In Vivo* and *Ex Vivo* Fluorescence Imaging.** All animal studies were performed in compliance with protocols that had been approved by the Hubei Provincial Animal Care and Use Committee and with the experimental guidelines of the Animal Experimentation Ethics Committee of Huazhong University of Science and Technology. The mRFP-5-8F cells (2×10^6 cells per site) were implanted subcutaneously into the hind flanks of mice. When the tumors reached 5−8 mm in diameter (2−3 weeks after implantation), 6 nmol of (DiR-BOA)α-NTP-LNs or (DiR-BOA)α-sNTP-LNs was intravenously injected into the tumor-bearing mice. *In vivo* and *ex vivo* fluorescence imaging of the mice and tissues was performed using a custom-made whole-body optical imaging system. Fluorescence images of DiR-BOA were acquired with a near-infrared filter set (excitation = 716/40 nm; emission = 775/46 nm) and calibrated with an autofluorescence background filter set (excitation = 562/40 nm; emission = 775/46 nm). Fluorescence images of mRFP were acquired with a deep red filter set (excitation = 562/40 nm; emission = 655/40 nm) and calibrated with an autofluorescence background filter set (excitation = 469/35 nm; emission = 655/40 nm).

Fluorescence Analysis of Frozen Slices and Suspended Cells from Tumor and Normal Tissues. The tumor-bearing mice were sacrificed by cervical dislocation 48 h after the nanoparticle injection. Tumor tissues were collected, sliced into 5 μm sections with a Shandon FSE cryotome (Thermo Scientific, Runcorn, UK), and then stained with Hoechst 33342. The frozen sections of tumor tissues were imaged using multispectral microscopy with a Nuance spectral imaging system (CRI, Woburn, MA). To compare the uptake efficiencies of the nanoparticles by the cells in tumor and normal tissues, organs (*e.g.*, liver, kidney, spleen, lung) were collected and dispersed into single-cell suspensions with superfine homogenizers (Fluko 6/10; Fluid Kotthoff GmbH, Essen, Germany). To quantify the uptake efficiency of nanoparticles by the cells in various tissues, the cell suspensions (tumor, liver, kidney, spleen, and lung) were analyzed by flow cytometry. Regions corresponding to cells were defined on the cytogram of forward light scatter (FSC) *versus* side-angle light scatter (SSC). In the quantitative analysis of the uptake of DiR-BOA-labeled nanoparticles, positive cells were defined by comparison with negative cells from normal organ (*e.g.*, kidney) in the dot plot (DiR-BOA *versus* SSC). The uptake efficiencies of DiR-BOA-labeled nanoparticles by the cells of various tissues are presented as the summed fluorescence intensity of the DiR-BOA-positive cells divided by the total number of gated cells (1×10^5).

Blood Clearance Kinetics. Five normal BALB/c mice were used as one group for the blood clearance test of fluorescent labeling of the nanoparticles (DiR-BOA)α-NTP-LNs and (DiR-BOA)α-sNTP-LNs. After intravenous administration of the nanoparticles, blood samples were collected from the orbital sinus at 10 min, 0.5, 1, 2, 3, 6, 12, 24, 36, and 48 h postinjection. The fluorescence intensity of DiR-BOA in the blood samples was measured using a spectrophotometer (Lambda 35; PerkinElmer, Waltham MA, USA) and recorded per milligram of blood. A fluorescence intensity *versus* time plot was used to determine the blood half-life of the nanoparticles.

Evaluation of the Inhibitory Effect of Nanoparticles on Tumor Growth. The 5-8F tumor-bearing mice were divided into four groups on day 4 after tumor cell implantation. Each group contained five mice, and the mice were intravenously injected with α-NTP-LNs, α-sNTP-LNs, α-NTP, or PBS on days 4 and 6, respectively. The dose of nanoparticles was equivalent to 250 nmol of peptide. As a negative control, HT1080 tumor-bearing mice were randomly divided into two groups that were intravenously injected with 250 nmol α-NTP-LNs and PBS, respectively. The tumor size was measured using a caliper. The volume was calculated as $V = (\pi/6 \times \text{longest diameter} \times \text{perpendicular diameter}^2)$.

Histopathological Analyses and Immunofluorescence. The tumors, livers, spleens, kidneys, and lungs were extracted from tumor-bearing mice and fixed in a 4% paraformaldehyde solution. The tumors and organs were embedded in paraffin, sectioned, and processed for hematoxylin and eosin (HE) staining, TdT-mediated dUTP nick end labeling (TUNEL), and fluorescence immunohistochemical staining with a rabbit anti-LC3B antibody (1:200) and an Alexa Fluor 594-labeled donkey anti-rabbit secondary antibody (1:400). The images for the HE staining and the TUNEL assay were acquired using a Nuance spectral imaging system with a 40× objective. The percentage of cells undergoing apoptosis was calculated as the ratio of apoptotic cells to total cells in 20 imaged fields from three tumors. The immunofluorescence signals of the LC3B dots were imaged using a Nikon A1 MP laser scanning confocal microscope with an excitation wavelength of 561 nm and a 60×/1.2 NA water immersion objective (image field = 512 × 512 pixels, 0.21 × 0.21 mm^2). The amount of LC3B dots was quantified by counting the number of fluorescence labeled LC3B dots or vacuoles, which were recognized using the cell counter function in ImageJ software (version 1.44, NIH, Bethesda, MD, USA; available on the Internet). The data were collected from at least 30 imaged fields from three mice and presented as the numbers of LC3B dots per square millimeter.

Blood Hemanalysis and Biochemical Analyses. Blood samples were collected from the mice before they were sacrificed on day 16 after tumor cell implantation. The blood cell and biochemical analyses were performed using a hematology analyzer (BC-3200, Mindray, Shenzhen, China) and an automatic biochemical analyzer (Spotchem EZ SP-4430, Arkray Inc., Kyoto, Japan), respectively.

Evaluation of the Prohibition of Nanoparticles on Tumor Metastasis. The 5-8F tumor cells (2×10^6) were intravenously injected into nude mice. On days 8 and 10 after tumor cell injection, the mice were intravenously injected with α-NTP-LNs, α-sNTP-LNs, α-NTP, or PBS. The dose of nanoparticles was equivalent to 250 nmol of peptide. On day 45, three mice of PBS control group and α-NTP-LN-treated group were sacrificed. HE staining of the lungs was performed. The survival time of each mouse was observed. The remaining mice in PBS control group ($n = 9$), α-NTP-LN-treated group ($n = 9$), α-sNTP-LN-treated group ($n = 5$), and α-NTP-treated group ($n = 5$) were observed for their survival time.

Statistics. All data are expressed as the mean ± SD. Nonparametric statistical tests (Kruskal−Wallis and Mann−Whitney U tests) were used to analyze the significance of the differences in the blood hemanalysis and biochemical parameters, and other data were analyzed by two-tailed Student's *t* tests. Differences between or among groups are labeled as n.s. for not significant, * for $P < 0.05$, ** for $P < 0.01$, and *** for $P < 0.001$. Graph Pad Prism with the log-rank test was used for the survival data analysis.

Conflict of Interest: The authors declare no competing financial interest.

Acknowledgment. We thank Dr. Gang Zheng (University of Toronto, Toronto, ON, Canada) for paper discussion. We thank Prof. Yi-Xin Zeng and Prof. Mu-Sheng Zeng of the Sun Yat-sen University Cancer Center for providing all nasopharyngeal cancer cell lines. We also thank the Optical Bioimaging Core Facility of WNLO-HUST for the support in data acquisition, the Center for Nanoscale Characterization & Devices (CNCD, Tecnai G^2 20 U-Twin) in WNLO-HUST for the facility support, and the Analytical and Testing Center of HUST for spectral

measurements. This work was supported by the National Basic Research Program of China (Grant No. 2011CB910401), Science Fund for Creative Research Group of China (Grant No. 61121004), National Natural Science Foundation of China (Grant No. 81172153), National Science and Technology Support Program of China (Grant No. 2012BAI23B02), and the seed project of WNLO.

Supporting Information Available: The absorption spectrum of FITC-(DiR-BOA)α-NTP-LNs. Seminative SDS-PAGE assay and fluorescence imaging to evaluate the stability of FITC-(DiR-BOA)α-NTP-LNs. Test of long-term size stability of α-NTP-LNs using dynamic light scattering. FPLC and DLS profiles of α-LNs and α-sNTP-LNs. Intracellular uptake of (DiR-BOA)α-NTP-LNs by 5-8F cells after various incubation times. Confocal imaging of the uptake of FITC-(DiR-BOA)α-NTP-LNs by 5-8F cells. Evaluation of the mobility and colony formation of 5-8F cells treated with 50 μM α-NTP-LNs or PBS. Fluorescence imaging analyses of the colocalization of DiR-BOA and mRFP in tumor sections that were prestained with DAPI (blue) before multispectral microscopy. Flow cytometric dot plot (DiR-BOA/SSC) of single-cell suspensions from tumor and representative normal organs (liver, kidney, spleen, and lung). Blood clearance curve of α-NTP in normal mice. *In vivo* evaluation of the effect of α-NTP-LNs on HT1080 tumor-bearing mice. Line plot of the body weight changes in 5-8F tumor-bearing mice treated with α-NTP-LNs, α-sNTP-LNs, α-NTP, or PBS. Evaluation of the side effects of α-NTP-LNs, α-sNTP-LNs, and α-NTP *in vivo*. Histological analysis of the lung metastasis of the NPC 5-8F tumor. Fusion peptide containing the NTP conjugated to the N-terminus of the α-peptide fail to form lipid nanoparticles. Flow cytometry analysis verified that the fluorescence intensity corresponding to FITC-α-NTP uptake by 5-8F cells was positively correlated with the cell death rate determined by propidium iodide labeling. This material is available free of charge *via* the Internet at http://pubs.acs.org.

REFERENCES AND NOTES

1. McDermott, A. L.; Dutt, S. N.; Watkinson, J. C. The Aetiology of Nasopharyngeal Carcinoma. *Clin. Otolaryngol.* **2001**, *26*, 82–92.
2. Wei, W. I.; Sham, J. S. T. Nasopharyngeal Carcinoma. *Lancet* **2005**, *365*, 2041–2054.
3. Mould, R. F.; Tai, T. H. Nasopharyngeal Carcinoma: Treatments and Outcomes in the 20th Century. *Br. J. Radiol.* **2002**, *75*, 307–339.
4. Liu, Q.; Chen, J. O.; Huang, Q. H.; Li, Y. H. Trends in the Survival of Patients with Nasopharyngeal Carcinoma between 1976 and 2005 in Sihui, China: A Population-Based Study. *Chin. J. Cancer* **2013**, *32*, 325–333.
5. Lee, A. W.; Sze, W. M.; Au, J. S.; Leung, S. F.; Leung, T. W.; Chua, D. T.; Zee, B. C.; Law, S. C.; Teo, P. M.; Tung, S. Y.; *et al.* Treatment Results for Nasopharyngeal Carcinoma in the Modern Era: The Hong Kong Experience. *Int. J. Radiat. Oncol. Biol. Phys.* **2005**, *61*, 1107–1116.
6. Ma, B. B.; Kam, M. K.; Leung, S. F.; Hui, E. P.; King, A. D.; Chan, S. L.; Mo, F.; Loong, H.; Yu, B. K.; Ahuja, A.; *et al.* A Phase II Study of Concurrent Cetuximab-Cisplatin and Intensity-Modulated Radiotherapy in Locoregionally Advanced Nasopharyngeal Carcinoma. *Ann. Oncol.* **2012**, *23*, 1287–1292.
7. Soo, R. A.; Wu, J.; Aggarwal, A.; Tao, Q.; Hsieh, W.; Putti, T.; Tan, K. B.; Low, J. S.; Lai, Y. F.; Mow, B.; *et al.* Celecoxib Reduces Microvessel Density in Patients Treated with Nasopharyngeal Carcinoma and Induces Changes in Gene Expression. *Ann. Oncol.* **2006**, *17*, 1625–1630.
8. Leemans, C. R.; Braakhuis, B. J. M.; Brakenhoff, R. H. The Molecular Biology of Head and Neck Cancer. *Nat. Rev. Cancer* **2011**, *11*, 9–22.
9. Chan, A. T.; Hsu, M. M.; Goh, B. C.; Hui, E. P.; Liu, T. W.; Millward, M. J.; Hong, R. L.; Whang-Peng, J.; Ma, B. B.; To, K. F.; *et al.* Multicenter, Phase II Study of Cetuximab in Combination with Carboplatin in Patients with Recurrent or Metastatic Nasopharyngeal Carcinoma. *J. Clin. Oncol.* **2005**, *23*, 3568–3576.
10. Burtness, B.; Goldwasser, M. A.; Flood, W.; Mattar, B.; Forastiere, A. A. Eastern Cooperative Oncology, G. Phase III Randomized Trial of Cisplatin Plus Placebo Compared with Cisplatin Plus Cetuximab in Metastatic/Recurrent Head and Neck Cancer: An Eastern Cooperative Oncology Group study. *J. Clin. Oncol.* **2005**, *23*, 8646–8654.
11. Davis, M. E.; Chen, Z. G.; Shin, D. M. Nanoparticle Therapeutics: An Emerging Treatment Modality for Cancer. *Nat. Rev. Drug Discovery* **2008**, *7*, 771–782.
12. Peer, D.; Karp, J. M.; Hong, S.; Farokhzad, O. C.; Margalit, R.; Langer, R. Nanocarriers as an Emerging Platform for Cancer Therapy. *Nat. Nanotechnol.* **2007**, *2*, 751–760.
13. Ferrari, M. Cancer Nanotechnology: Opportunities and Challenges. *Nat. Rev. Cancer* **2005**, *5*, 161–171.
14. Ng, K. K.; Lovell, J. F.; Zheng, G. Lipoprotein-Inspired Nanoparticles for Cancer Theranostics. *Acc. Chem. Res.* **2011**, *44*, 1105–1113.
15. Ashley, C. E.; Carnes, E. C.; Phillips, G. K.; Padilla, D.; Durfee, P. N.; Brown, P. A.; Hanna, T. N.; Liu, J.; Phillips, B.; Carter, M. B.; *et al.* The Targeted Delivery of Multicomponent Cargos to Cancer Cells by Nanoporous Particle-Supported Lipid Bilayers. *Nat. Mater.* **2011**, *10*, 389–397.
16. Nel, A. E.; Madler, L.; Velegol, D.; Xia, T.; Hoek, E. M. V.; Somasundaran, P.; Klaessig, F.; Castranova, V.; Thompson, M. Understanding Biophysicochemical Interactions at the Nano-Bio Interface. *Nat. Mater.* **2009**, *8*, 543–557.
17. Desai, N. Challenges in Development of Nanoparticle-Based Therapeutics. *AAPS J.* **2012**, *14*, 282–295.
18. Shadidi, M.; Sioud, M. Identification of Novel Carrier Peptides for the Specific Delivery of Therapeutics into Cancer Cells. *FASEB J.* **2003**, *17*, 256–258.
19. Wang, X. F.; Birringer, M.; Dong, L. F.; Veprek, P.; Low, P.; Swettenham, E.; Stantic, M.; Yuan, L. H.; Zobalova, R.; Wu, K.; *et al.* A Peptide Conjugate of Vitamin E Succinate Targets Breast Cancer Cells with High ErbB2 Expression. *Cancer Res.* **2007**, *67*, 3337–3344.
20. Luo, H. M.; Yang, J.; Jin, H. L.; Huang, C.; Fu, J. W.; Yang, F.; Gong, H.; Zeng, S. Q.; Luo, Q. M.; Zhang, Z. H. Tetrameric Far-Red Fluorescent Protein as a Scaffold To Assemble An Octavalent Peptide Nanoprobe for Enhanced Tumor Targeting and Intracellular Uptake *in Vivo*. *FASEB J.* **2011**, *25*, 1865–1873.
21. Luo, H.; Shi, J.; Jin, H.; Fan, D.; Lu, L.; Wang, F.; Zhang, Z. An (125)I-Labeled Octavalent Peptide Fluorescent Nanoprobe for Tumor-Homing Imaging *in Vivo*. *Biomaterials* **2012**, *33*, 4843–4850.
22. Zhang, Z.; Cao, W.; Jin, H.; Lovell, J. F.; Yang, M.; Ding, L.; Chen, J.; Corbin, I.; Luo, Q.; Zheng, G. Biomimetic Nanocarrier for Direct Cytosolic Drug Delivery. *Angew. Chem., Int. Ed.* **2009**, *48*, 9171–9175.
23. Lin, Q.; Chen, J.; Ng, K. K.; Cao, W.; Zhang, Z.; Zheng, G. Imaging the Cytosolic Drug Delivery Mechanism of HDL-like Nanoparticles. *Pharm. Res.* **2013**, 10.1007/s11095-013-1046-z.
24. Zheng, Y.; Liu, Y.; Jin, H.; Pan, S.; Qian, Y.; Huang, C.; Zeng, Y.; Luo, Q.; Zeng, M.; Zhang, Z. Scavenger Receptor B1 Is a Potential Biomarker of Human Nasopharyngeal Carcinoma and Its Growth Is Inhibited by HDL-Mimetic Nanoparticles. *Theranostics* **2013**, *3*, 477–486.
25. Yang, M.; Chen, J.; Cao, W. G.; Ding, L. L.; Ng, K. K.; Jin, H. L.; Zhang, Z. H.; Zheng, G. Attenuation of Nontargeted Cell-Kill Using a High-Density Lipoprotein-Mimicking Peptide Phospholipid Nanoscaffold. *Nanomedicine* **2011**, *6*, 631–641.
26. Corbin, I. R.; Chen, J.; Cao, W.; Li, H.; Lund-Katz, S.; Zheng, G. Enhanced Cancer-Targeted Delivery Using Engineered High-Density Lipoprotein-Based Nanocarriers. *J. Biomed. Nanotechnol.* **2007**, *3*, 367–376.
27. Zhang, Z.; Chen, J.; Ding, L.; Jin, H.; Lovell, J. F.; Corbin, I. R.; Cao, W.; Lo, P. C.; Yang, M.; Tsao, M. S.; *et al.* HDL-Mimicking Peptide-Lipid Nanoparticles with Improved Tumor Targeting. *Small* **2010**, *6*, 430–437.
28. Baehrecke, E. H. Autophagy: Dual Roles in Life and Death? *Nat. Rev. Mol. Cell Biol.* **2005**, *6*, 505–510.

29. Yokoyama, T.; Tam, J.; Kuroda, S.; Scott, A. W.; Aaron, J.; Larson, T.; Shanker, M.; Correa, A. M.; Kondo, S.; Roth, J. A.; *et al.* EGFR-Targeted Hybrid Plasmonic Magnetic Nanoparticles Synergistically Induce Autophagy and Apoptosis in Non-Small Cell Lung Cancer Cells. *PLoS One* **2011**, *6*, e25507.
30. Kuma, A.; Matsui, M.; Mizushima, N. LC3, an Autophagosome Marker, Can Be Incorporated into Protein Aggregates Independent of Autophagy. *Autophagy* **2007**, *3*, 323–328.
31. Gozuacik, D.; Kimchi, A. Autophagy as a Cell Death and Tumor Suppressor Mechanism. *Oncogene* **2004**, *23*, 2891–2906.
32. Wang, L.; Chen, M.; Yang, J.; Zhang, Z. LC3 Fluorescent Puncta in Autophagosomes or in Protein Aggregates Can Be Distinguished by FRAP Analysis in Living Cells. *Autophagy* **2013**, *9*, 756–769.
33. Kabeya, Y.; Mizushima, N.; Uero, T.; Yamamoto, A.; Kirisako, T.; Noda, T.; Kominami, E.; Ohsumi, Y.; Yoshimori, T. LC3, a Mammalian Homologue of Yeast Apg8p, Is Localized in Autophagosome Membranes after Processing. *EMBO J.* **2000**, *19*, 5720–5728.
34. Yang, X.; Gong, H.; Fu, J.; Quan, G.; Huang, C.; Luo, Q. Molecular Imaging of Small Animals with Fluorescent Proteins: From Projection to Multimodality. *Comput. Med. Imaging Graph.* **2012**, *36*, 259–263.
35. Xiong, T.; Zhang, Z.; Liu, B. F.; Zeng, S.; Chen, Y.; Chu, J.; Luo, Q. *In Vivo* Optical Imaging of Human Adenoid Cystic Carcinoma Cell Metastasis. *Oral Oncol.* **2005**, *41*, 709–715.
36. Yang, M.; Jin, H. L.; Chen, J. A.; Ding, L. L.; Ng, K. K.; Lin, Q. Y.; Lovell, J. F.; Zhang, Z. H.; Zheng, G. Efficient Cytosolic Delivery of siRNA Using HDL-Mimicking Nanoparticles. *Small* **2011**, *7*, 568–573.
37. Lin, Q. Y.; Chen, J.; Jin, H. L.; Ng, K. K.; Yang, M.; Cao, W. G.; Ding, L. L.; Zhang, Z. H.; Zheng, G. Efficient Systemic Delivery of siRNA by Using High-Density Lipoprotein-Mimicking Peptide Lipid Nanoparticles. *Nanomedicine* **2012**, *7*, 1813–1825.
38. Jin, H. L.; Lovell, J. F.; Chen, J.; Ng, K.; Cao, W. G.; Ding, L. L.; Zhang, Z. H.; Zheng, G. Cytosolic Delivery of LDL Nanoparticle Cargo Using Photochemical Internalization. *Photochem. Photobiol. Sci.* **2011**, *10*, 810–816.
39. Huang, C.; Jin, H.; Qian, Y.; Qi, S.; Luo, H.; Luo, Q.; Zhang, Z. Hybrid Melittin Cytolytic Peptide-Driven Ultrasmall Lipid Nanoparticles Block Melanoma Growth *in Vivo*. *ACS Nano* **2013**, *7*, 5791–5800.
40. Xu, H. N.; Zhao, H.; Mir, T. A.; Lee, S. C.; Feng, M.; Choe, R.; Glickson, J. D.; Li, L. Z. Chop Therapy Induced Mitochondrial Redox State Alteration in Non-Hodgkin's Lymphoma Xenografts. *J. Innovative Opt. Health Sci.* **2013**, *6*, 1350011.
41. Axe, E. L.; Walker, S. A.; Manifava, M.; Chandra, P.; Roderick, H. L.; Habermann, A.; Griffiths, G.; Ktistakis, N. T. Autophagosome Formation from Membrane Compartments Enriched in Phosphatidylinositol 3-Phosphate and Dynamically Connected to the Endoplasmic Reticulum. *J. Cell Biol.* **2008**, *182*, 685–701.